JOURNAL OF GEOPHYSICAL RESEARCH, VOL. 99, NO. A2, PAGES 2261–2270, FEBRUARY 1, 1994

A revised analysis of micron-sized particles detected near Saturn by the Voyager 2 plasma wave instrument

D. Tsintikidis, D. Gurnett, L. J. Granroth, S. C. Allendorf, and W. S. Kurth
Department of Physics and Astronomy, University of Iowa, Iowa City

Abstract. The impulsive noise that the plasma wave and radio astronomy instruments detected during the Voyager 2 swing by Saturn was attributed to dust grains striking the spacecraft. This report presents a reanalysis of the dust impacts recorded by the plasma wave instrument using an improved model for the response of the electric antenna to dust impacts. The fundamental assumption used in this analysis is that the voltage induced on the antenna is proportional to the mass of the impacting grain. Using the above assumption and the antenna response constants used at Uranus and Neptune, the following conclusions can be reached. The primary dust distribution consists of a "disk" of particles that coincides with the equator plane and has a north-south thickness of $2\Delta z = 962$ km. A less dense "halo" with a north-south thickness of $2\Delta z = 3376$ km surrounds the primary distribution. The dust particle sizes are of the order of 10 μm, assuming a mass density of 1 g/cm^3. The corresponding particle masses are of the order of 10^{-9} g, and maximum number densities are of the order of 10^{-2} m^{-3}. Most likely, the G ring is the dominate source since the particles were observed very close to that ring, namely at 2.86 R_S. Other sources, like nearby moons, are not ruled out especially when perturbations due to electromagnetic forces are included. The calculated optical depth differs by about a factor of 2 from photometric studies. The current particle masses, radii, and the effective north-south thickness of the particle distribution are larger than what Gurnett et al. (1983) reported by about 2, 1, and 1 orders of magnitude, respectively. This is attributed to the fact that the collection coefficient used in this study is smaller than what was used in Gurnett et al.'s earlier publication.

1. Introduction

On August 26, 1981, the Voyager 2 spacecraft made a close pass by the planet Saturn. The spacecraft crossed the ring plane at a radial distance of 2.86 R_S, very close to the G ring. Both the plasma wave and the planetary radio astronomy instruments detected a region of very intense and impulsive noise near the ring plane crossing [*Scarf et al.*, 1982; *Warwick et al.*, 1982]. This noise is similar to noise later detected during the ring plane crossing at Uranus and Neptune [*Gurnett et al.*, 1987, 1991; *Meyer-Vernet et al.*, 1986; *Pedersen et al.*, 1991]. The spectrum of this noise extended upward to frequencies certainly above the local electron plasma frequency. *Warwick et al.* [1982] reported that the planetary radio astronomy (PRA) instrument on Voyager 2 also detected an intense event at or near the time of the ring plane crossing. At its peak the event extended from frequencies of 10 Hz or less to approximately 1 MHz. Thus it was concluded that this noise could not be attributed to plasma waves. Since the noise was of an impulsive nature and the spacecraft was close to the ring plane, the conclusion was drawn that the noise was produced by impacts of particles hitting the spacecraft. The signal is caused by an impact ionization effect that occurs when very small dust grains strike the spacecraft at high velocities. When the dust grain strikes the spacecraft at a relative velocity greater than a few kilometers per second, the grain is instantly vaporized and is heated to a temperature in excess of 10^5 °K. A small, partially ionized cloud of gas is produced that expands outwardly from the point of impact. This cloud of ionized gas is detected by the electric antenna. Making assumptions about the charge yield and the coupling efficiency of the cloud to the antenna, it is possible to estimate the mass and the size of the impacting particles. This is accomplished by studying the amplitude of the voltage pulse on the antenna. By knowing also the spacecraft velocity and its cross-sectional area, the number density of the particles can also be computed.

The phenomenon of the dust impacts at Saturn was first studied in detail by *Gurnett et al.* [1983]. The method used in that study for estimating the collection coefficient α was highly uncertain. The collection coefficient is directly related to the voltage detected by the antennas and is a crucial parameter. In the analysis of the Uranus and Neptune data, *Gurnett et al.* [1987, 1991] applied an improved method based on comparisons with the planetary radio astronomy instrument to provide better estimates of the coupling efficiency. In this report we use the same method (see section 3) to reanalyze the Saturn dust impact data. The purpose of this report is to give (1) a detailed description of the impact-generated signals, (2) an interpretation of the impact noise in terms of the particles' masses and sizes as well as their number densities, (3) a discussion of the possible sources of the particles, and (4) a comparison of the new results with the old results of *Gurnett et al.* [1983].

Paper number 93JA02906.
0148-0227/94/93JA-02906$05.00

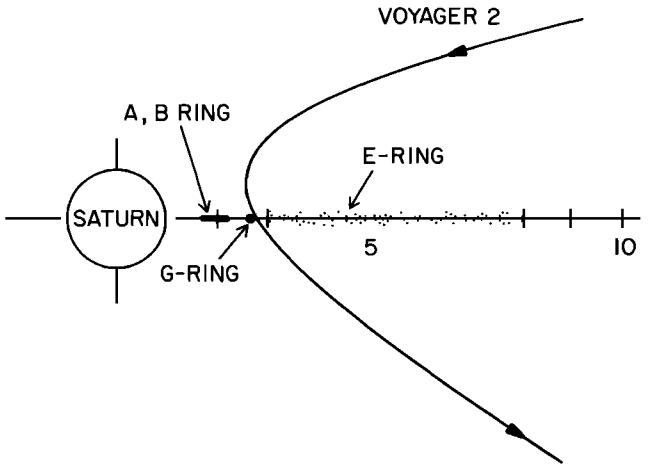

Figure 1. The path of Voyager 2 as it appears to be in a meridional plane coinciding with the spacecraft trajectory plane. Voyager 2 crossed the ring plane at 2.86 R_S, very close to the G ring. The E ring dimensions have been magnified for clarity purposes.

2. Observations

A good first step before discussing the observations is to review the operation of the plasma wave instrument (PWS). The plasma wave instrument utilizes two antenna elements, each 10 m long and 1.3 cm in diameter. The elements are mounted in a V configuration at an angle of 90° with respect to each other. The plasma wave instrument uses the two elements as a dipole (resulting in a 7-m effective antenna length), which means that the instrument responds to the voltage difference between the two elements. This is different from the way the antennas are utilized by the planetary radio astronomy experiment. In the latter case the antennas are used as monopoles, which means that they respond to the voltage difference between the elements and the spacecraft body. The difference in the instrument response will be useful later in the interpretation of the impact signals.

Voltage signals from the antennas are processed in two ways by the plasma wave instrument. First, a 16-channel spectrum analyzer is used to provide absolute voltage intensities in 16 frequency channels from 10 Hz to 56 kHz. There are four channels per decade (i.e., 10.0, 17.8, 31.1, and 56.2 Hz), and their bandwidth is about 10% of the center frequency. Second, a wideband waveform receiver is used to provide waveforms during selected periods between 50 Hz and 10 kHz. The sampling rate is 28,800 4-bit samples per second. Typically, the data waveforms are obtained in 48-s intervals or frames, with each frame containing 800 successive 55.55-ms data blocks. The sampling rate corresponds to 34.7 μs between samples. An automatic gain control (AGC) is included in the wideband receiver whose function is to maintain a nearly constant output signal amplitude. The AGC time constant is 0.5 s. Although the automatic gain control destroys information about absolute amplitude, the resulting waveform gives information about relative amplitudes. For a more complete description of the plasma wave instrument, see *Scarf and Gurnett* [1977].

As is shown in Figure 1, Voyager 2 passed through the ring plane close to the planet, just beyond the G ring. The ring plane crossing occurred at 0418:16 spacecraft event time (SCET) on August 26, 1981, at a radial distance of 2.86 Saturnian radii (1 R_S = 60,330 km). During the crossing a very intense burst of noise was detected by both the plasma wave and radio astronomy instruments. The maximum intensity occurred almost exactly at the ring plane crossing. The electric field intensities can be seen in Figure 2. Figure 2 shows the intensities in each individual channel of the 16-channel spectrum analyzer. The dust impact noise consists of the sharply peaked feature at approximately 4 hours 18 min. This feature has essentially the same shape as the dust features in Uranus and Neptune. The root-mean-square (rms) antenna voltage V_{rms}, obtained by integrating across all channels, is 0.137 volts, which is one of the highest values ever recorded by the Voyager plasma wave instrument. This value is smaller by a factor of 2 than the value originally published by *Gurnett et al.* [1983]. This change is attributed to a small adjustment in the calibration of the plasma wave instrument that occurred after the initial report was published. However, the main features are virtually the same. As can be seen in Figure 2, the signature of the noise intensity is well defined around the ring plane crossing and exhibits the same characteristics of the noise detected near the ring planes of the two outermost planets. The voltage spectrum at the time of maximum intensity is shown in Figure 3. As can be seen, the spectrum varies as f^{-4} at the higher frequencies, as was shown to be the case with the planetary radio astronomy instrument for all three outer planet encounters. For more details, see *Aubier et al.* [1983], *Meyer-Vernet et al.* [1986], and *Pedersen et al.* [1991].

The most convincing evidence that the noise detected was caused by dust impacts came from the wideband receiver. Since it was suspected that dust might be detected near the equator, a series of 48-s wideband frames was scheduled near the equator crossing. The locations and times of the frames are shown at the top of Figure 2. The importance of the wideband frames lies in the fact that individual dust impacts can be seen in the antenna voltage waveforms. A representative wideband waveform is shown in Figure 4. The impact waveform typically consists of an abrupt pulse followed by a complex oscillatory recovery (ringing effect) lasting up to several milliseconds. The risetime of the pulse is approximately 20–30 microseconds, which is of the same order of magnitude of the risetime of the 12-kHz low-pass filter of the wideband receiver.

A few comments would be appropriate about the pulses and how they are recorded by the wideband receiver. Many of the pulses are of small magnitude, thereby falling well within the instantaneous dynamic range of the receiver. However, many of the pulses are stronger and cause clipping as is evidenced in Figures 4c and 4d. The time constant of the automatic gain control is a half second, which is too slow to adjust to the rapid changes of the intensity of the impacts. The automatic gain control responds only to the average signal amplitude. The clipped waveforms are caused by saturation in the receiver. The true waveform is probably best represented by unclipped pulses, i.e., Figures 4a and 4b. The waveform typically exhibits a very rapid rise, with the first peak lasting a few tenths of a millisecond, followed by a somewhat longer second peak of opposite polarity that lasts from a large fraction of 1 ms to several milliseconds. *Sheehan et al.* [1994] presented laboratory results demonstrating the interaction of a small expanding plasma cloud with a simple antenna. These results corroborate the fact

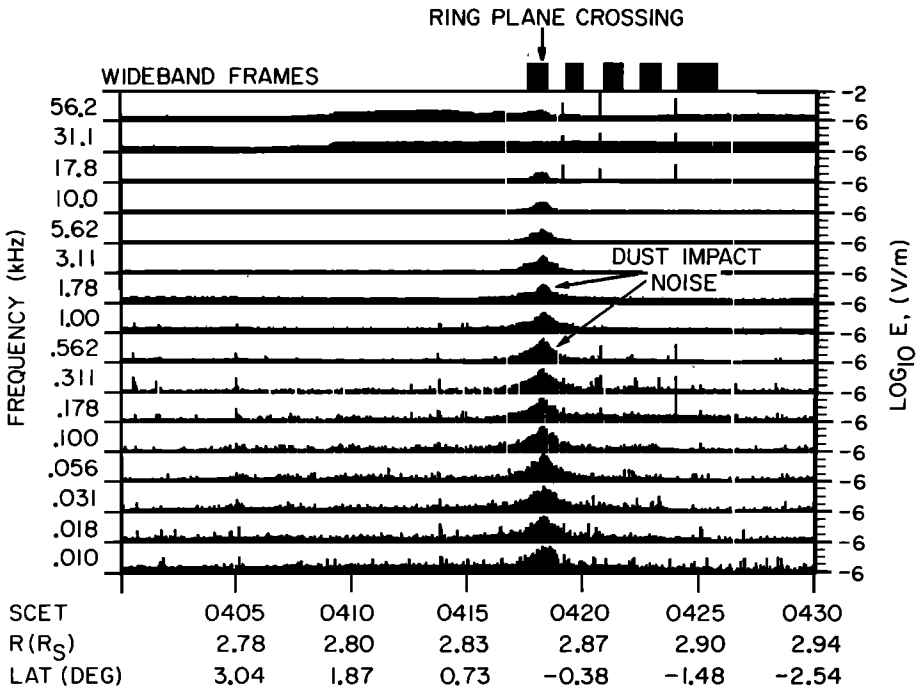

Figure 2. The electric field intensities measured by the 16-channel spectrum analyzer near the equatorial plane. The very intense broadband noise observed almost exactly at the equator crossing is attributed to particles hitting the spacecraft.

that the pulses can be attributed to expanding plasma clouds that originate from dust impacts. Mention should also be made of the fact that the wideband waveform data give information about the occurrence of an impact and nothing else. The broadband waveforms can be Fourier transformed to produce a spectrum similar to the several representatives seen in Figure 5. At high frequencies the spectral density decreases with increasing frequency as f^{-2}. The clipped impulses can be approximated as square waveforms. It can be shown that the power spectrum of such a waveform goes as f^{-2} [*Lee*, 1960], a fact which is consistent with the slope of the lines in Figure 5. The observed peak at approximately 100 Hz is believed to arise because of the recovery wave-

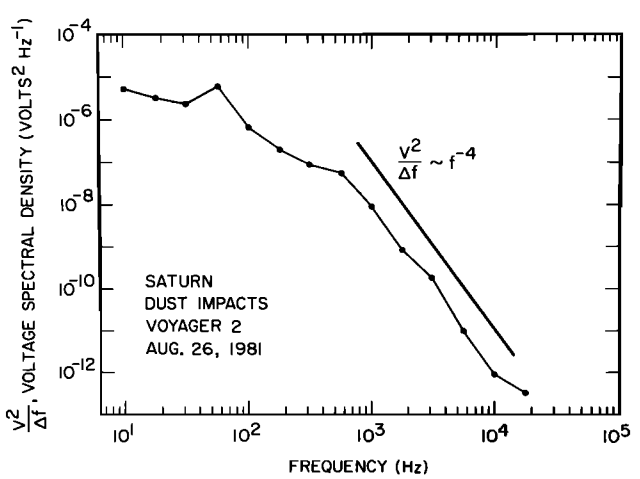

Figure 3. The voltage spectral density of the dust impact noise as recorded by the plasma wave instrument close to the time of maximum intensity at the ring plane crossing. It varies as f^{-4} at frequencies higher than a few hundred hertz, which is consistent with the results of the Uranus and Neptune encounters.

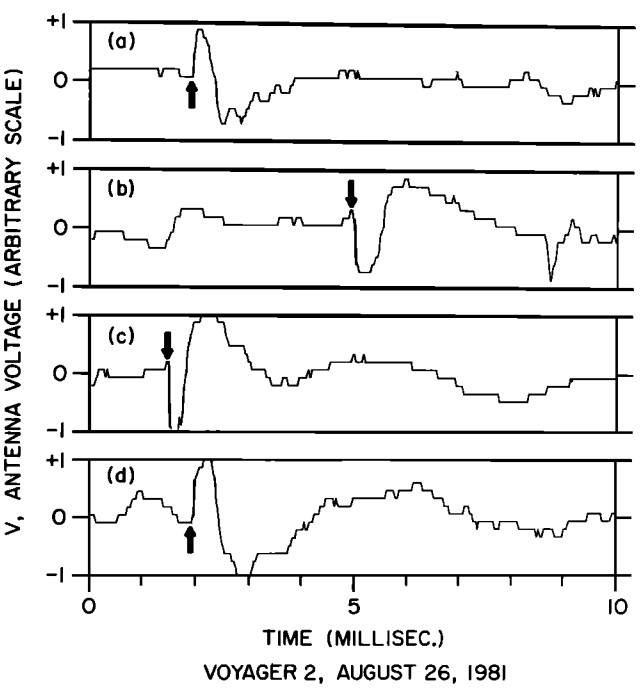

Figure 4. A series of dust impact waveforms in the vicinity of the ring plane crossing. The impacts are shown by arrows.

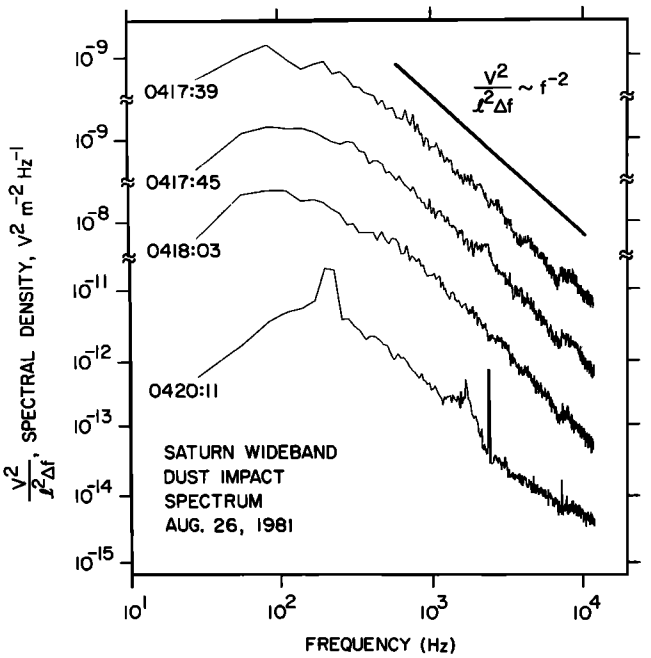

Figure 5. Selected frequency spectra of the broadband waveform data near the ring plane crossing. The f^{-2} voltage spectrum behavior at higher than a few hundred hertz is believed to be an instrument effect caused by the square-wavelike waveform that occurs during the recovery phase following large impacts.

form, which is dominated by frequency components in that range. Comparison of the results shown in Figure 5 with the results of Uranus and Neptune [see *Gurnett et al.*, 1987, 1991] shows that the spectra and waveforms are very similar.

3. Coupling Mechanisms

Possible coupling mechanisms between the dust impact and the electric antenna were discussed by *Gurnett et al.* [1983]. It was concluded that only impact ionization can produce the observed pulse amplitudes. Impact ionization is fairly well understood. When a small particle hits a solid surface at a sufficiently high velocity, the particle and part of the surface material are vaporized and heated to an extremely high temperature, 10^5 °K. Owing to the high temperature, some of the gas is ionized, thereby producing a small plasma cloud that expands away from the impact site, as illustrated in Figure 6. Various laboratory experiments have been performed to investigate impact ionization [i.e., *McDonnell*, 1978; *Fechtig et al.*, 1978; *Grün*, 1984]. The results show that to a good approximation the charge Q released during the impact is proportional to the mass m of the impacting particle,

$$Q = km, \tag{1}$$

where k is a yield constant that depends on both the velocity of the particle and the composition of both the particle and the target. In the case of Saturn it was shown that $k = 0.21$ C/g. However, caution should be exercised. This yield constant can only be regarded as a rough estimate, since there are uncertainties in the particle structure and composition, and other unknown factors might cause variations of as much as a factor of 10.

The next issue under consideration is the coupling of the charge pulse to the electric antenna. It is known that the impacts detected occur primarily on the spacecraft body and not on the antennas. Since the wideband waveforms respond to the voltage difference between the two antennas if the impacts detected were only on the antennas, then the ratio of the different pulse polarities should correspond to the ratio

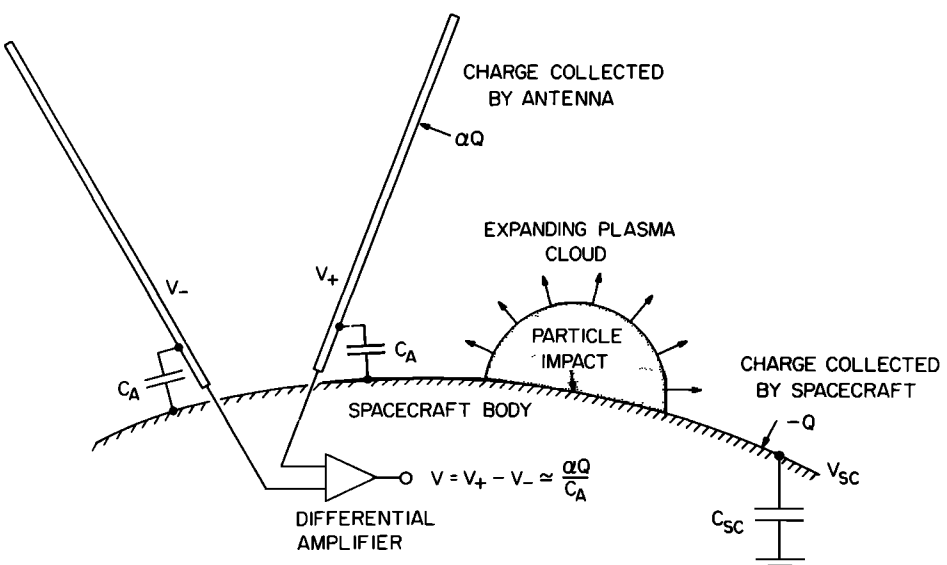

Figure 6. Schematic illustration of the model used to analyze the voltage produced by an impact. The spacecraft body collects the charge $-Q$ released by the impact, and the antenna collects a fraction α of it αQ. The voltage pulse produced is $V = \alpha Q/C_A$, where C_A is the antenna capacity, and it is detected by the antenna. Since the plasma wave instrument is a differential system, it does not respond to the charge collected by the spacecraft body.

of the projected antenna areas. During the Saturn ring plane crossing the ratio of the projected antenna areas was $A_1/A_2 = 1.82$. However, the ratio of the number of positive pulses to the number of negative pulses was $R_+/R_- = 1.13$. Since, to within the statistical uncertainty involved, the first ratio does not correspond to the second ratio, it was concluded that most of the impacts must be taking place on the spacecraft body. The polarity of each pulse is believed to be determined by the relative proximity of the impact site to the two antennas, meaning that the antenna closest to the impact site receives the largest perturbation.

In our study the amplitude of the voltage pulse is calculated assuming that a fraction α of the emitted charge Q is collected by one of the antennas, thereby producing a pulse of amplitude

$$V = \alpha \frac{Q}{C_A}, \tag{2}$$

where C_A is the antenna capacity and $C_A = 90$ pF. The above relationship is illustrated schematically in Figure 6. Since the risetime of the pulse is very fast (of the order of microseconds), a good case can be made that the charge collected by the antennas is due to electrons. The travel time of ions from the spacecraft body to the antennas is of the order of milliseconds, which is too long to account for the observed risetimes.

Besides the two antennas the spacecraft body can be a very efficient collector of charge, since the plasma cloud is formed very near its surface. In the ideal case of a differential measurement the plasma wave instrument should not respond to a voltage pulse on the spacecraft body. However, a response signal does occur because of imbalances in the antenna and the differential amplifier, but *Gurnett et al.* [1987] showed that the response signal is much smaller than the pulse amplitude given by (2). Hence only the antenna charge collection mechanism was considered in the present study.

Since the collection coefficient depends on the potential of the antenna as well as other unknown factors, such as the location of the impact, it is very difficult to estimate the collection coefficient α from fundamental principles. The collection coefficient initially was estimated to be possibly as high as 0.60 [*Gurnett et al.*, 1983], but the method used was uncertain. On the basis of the overlap in the dust impact spectra in the PWS and PRA data, *Gurnett et al.* [1987] later used the PRA data to calibrate the effective collection coefficient. The charge collection coefficient calculation was based on the fact that the signal resulting from the charge collected by the spacecraft body is much smaller than the signal resulting from the charge collected by the spacecraft antennas. Since the PRA instrument uses the antennas as two monopoles, the PRA data are inherently easier to interpret. Even if the general form and slope of the spectra are similar, the PWS intensities are seen to be much lower than the PRA intensities. The collection coefficient was defined as

$$\alpha = \frac{V_{\mathrm{PWS}}}{V_{\mathrm{PRA}}} \frac{C_A}{C_{sc}}, \tag{3}$$

where the ratio $V_{\mathrm{PWS}}/V_{\mathrm{PRA}}$ is the offset in the voltage spectrum, C_A is the antenna capacitance and $C_A = 90$ pF, and C_{sc} is the spacecraft capacitance and $C_{sc} = 330$ pF. Four values of α were computed corresponding to the ring plane crossings by Voyager 2 (one for Saturn, one for Uranus, and two for Neptune since there was an inbound and an outbound crossing). The results are summarized in Table 1. The average of the four values is 0.0078 ± 0.0011. The various values of α and the offsets can be seen in Figures 7a–7d. It should be noted that the collection coefficient represents an average over many impacts and is not applicable to any individual impact, since the antenna response depends in a complicated way on the location of the impact site which is unknown.

Table 1. Voyager 2 Offset Values, Charge Collection Coefficients, and Their Uncertainties for the Outer Three Planetary Encounters

Planet	$V_{\mathrm{PWS}}/V_{\mathrm{PRA}}$	α_{eff}	σ_{eff}
Saturn	0.0202	0.0055	0.0007
Uranus	0.0242	0.0066	0.0018
Neptune, inbound	0.0367	0.0100	0.0006
Neptune, outbound	0.0334	0.0091	0.0016

$V_{\mathrm{PWS}}/V_{\mathrm{PRA}}$ is the offset in voltage spectrum between the plasma wave (PWS) and planetary radio astronomy (PRA) instruments; α_{eff} is the charge collection coefficient; and σ_{eff} is the associated error.

The orientation of the spacecraft changed in each ring plane crossing. If the orientation of the spacecraft is such that most impacts occur near the antenna elements, then the plasma wave instrument will record large voltages. If the impacts occur away from the antennas, then less charge will be detected by the antennas. If the spread in the α values within the various ring plane crossings agrees with the spread in α for all the ring plane crossings, this is an indication that the charge collection mechanism is not affected by the orientation of the spacecraft. However, if the spreads vary, then the orientation of the spacecraft influences the outcome.

The following error analysis was performed in order to compare the spread in α and hence decide if the orientation of the spacecraft affects the estimation of α. The function S was defined for the Saturn ring plane crossing:

$$S = \frac{V}{(\Delta f)^{1/2}} f^2, \tag{4}$$

where $V/(\Delta f)^{1/2}$ is the Saturn PWS or PRA voltage value indicated with crosses or squares, respectively, in Figure 7a and f is the frequency that corresponds to the voltage value. Next the function S was calculated for each of the PWS and PRA points (crosses and squares, respectively) that are along the solid lines in Figure 7a. An average function S and its associated error were found next for both the PWS and PRA points, namely S_{PWS} and S_{PRA}. The ratio of the two is, in fact, the offset between the voltage spectra. Equation (3) provided the charge collection coefficient. The same procedure was repeated for the other ring plane crossings (Figures 7b–7d). The offsets, the charge collection coefficients, and the associated errors for each case can be seen in Table 1. Clearly, the spread of α within the various ring plane crossings varies during the different ring plane crossings

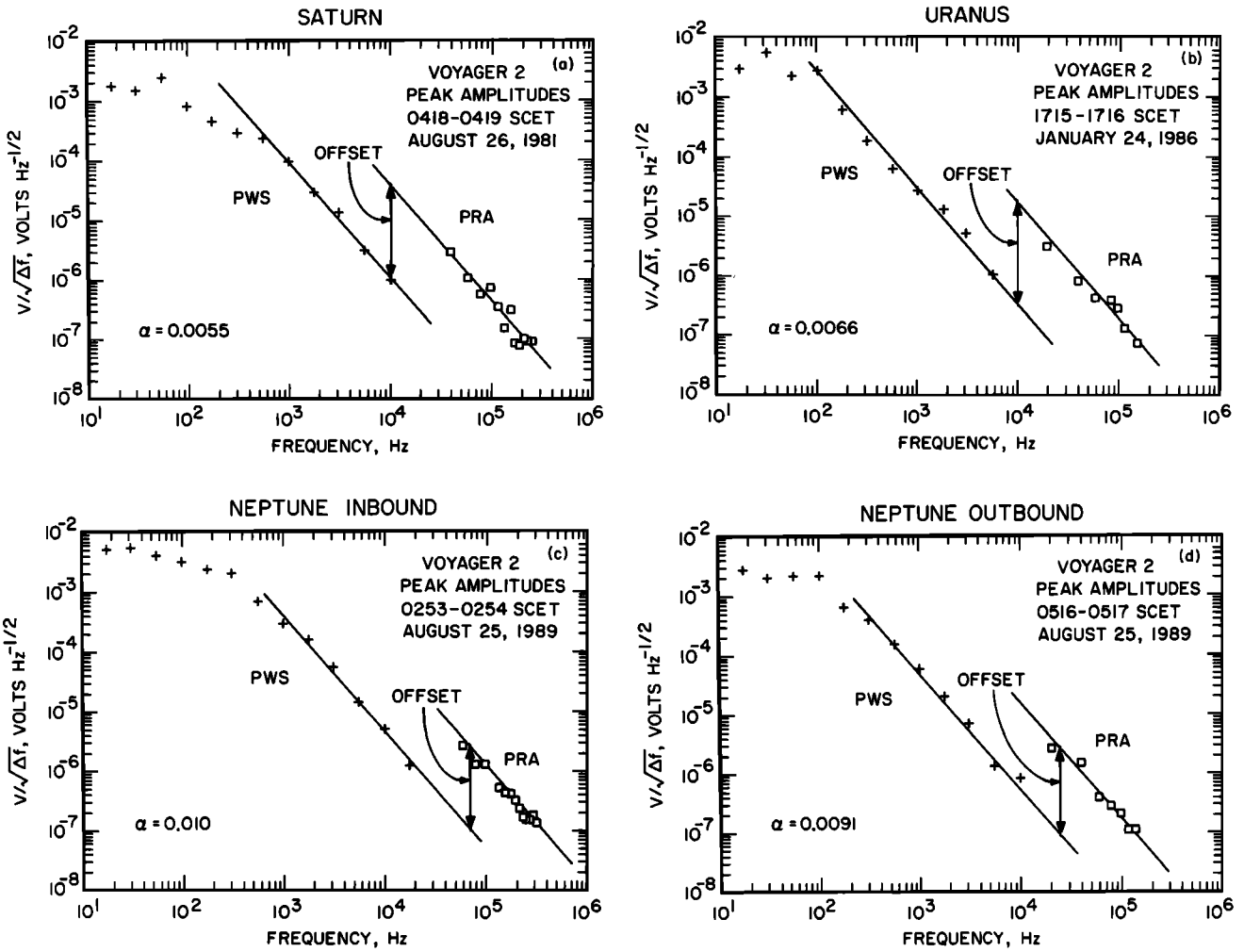

Figure 7. Comparison of the voltage spectra detected by the plasma wave (PWS) and planetary radio astronomy (PRA) instruments for the three outermost planetary encounters, (a) Saturn, (b) Uranus, (c) Neptune inbound, and (d) Neptune outbound. The charge collection coefficient α for each case can be seen in the lower left corner of each panel. The average α is $\bar{\alpha} = 0.0078$. The almost constant offset is caused by the different mode of electric field detection used by the two instruments (dipole and monopole, respectively, for PWS and PRA).

probably because the spacecraft orientation is different for each crossing thus influencing the charge collection coefficient. This error analysis provides a clear indication that the average value for the charge collection coefficient cannot be used. Instead, the value calculated for Saturn is better to use, hence the value of $\alpha = 0.0055$ is going to be used throughout this study.

4. Impact Rate, Number Density, and Particle Mass

One of the basic quantities that can be obtained from the waveform data is the impact rate R. By visually inspecting waveforms similar to the ones in Figure 4, it is possible to count individual impacts and thereby deduce the impact rate. In order to provide a good comparison with Uranus and Neptune, the same computer algorithm that was used in the previous dust studies was utilized again. The algorithm calculates the change between each successive pair of waveform samples and requires the slope of the sum of the two measurements to exceed a preset threshold. The counting threshold is adjusted in such a way as to give good agreement with visual identification of events shown in Figure 4. Since the slope criterion often generated false events during the oscillatory recovery phase, especially for strongly clipped waveforms, a dead time t_D was introduced after each event. The dead time is adjusted to be longer for events with steeper slopes, since the receiver takes longer to recover after larger events. The true counting rate R is then calculated from the observed counting rate R', using the following formula and correcting for dead time,

$$R = \frac{R'}{1 - \bar{t}_D R'}, \tag{5}$$

where $\bar{t}_D$ is the average dead time of 1.6 ms. The maximum counting rate was reached almost at the time of the equatorial plane crossing and is $R = 334\ \mathrm{s}^{-1}$. The impact rate profile, corrected for dead time, is shown in Figure 8. A well-defined peak can be seen near the equatorial plane ($z = 0$). Making the assumption that the particle distribution depends only on the distance z from the equatorial plane,

then the impact rate can be fit to a combination of Gaussian curves. For the case under study the following function gives a good fit (solid line in Figure 8),

$$R = R_0 + R_1 \exp\left[\frac{-(z-h)^2}{\Delta z_1^2}\right] + R_2 \exp\left[\frac{-(z-h)^2}{\Delta z_2^2}\right], \tag{6}$$

where h is the offset from the equatorial plane and Δz is the half thickness of the respective Gaussian component. The fit parameters are $R_0 = 23 \pm 1\ s^{-1}$, $R_1 = 262 \pm 7\ s^{-1}$, $R_2 = 50 \pm 5\ s^{-1}$, $h = 8 \pm 9$ km, $\Delta z_1 = 481 \pm 15$ km, and $\Delta z_2 = 1688 \pm 129$ km.

The optimum values of the fit parameters were obtained by minimizing the goodness of fit x^2 with respect to each of the parameters simultaneously. In the process of performing the minimization, it was judged visually that two Gaussian functions gave a better fit than if only one Gaussian was used. The associated error of each parameter was defined to be the product of the error of each data point multiplied by the effect which that data point had on the determination of the parameter. For a complete description on error analysis, see *Press et al.* [1989].

Having found the impact rate and using the antenna coupling model discussed in the previous section, we proceed to the next step, which is to estimate the number density and the mass of the impacting particles. The number density n is given by

$$R = nUA_{sc}, \tag{7}$$

where A_{sc} is the effective cross-sectional area of the spacecraft body and U is the relative speed between the spacecraft and the particles. The effective cross-sectional area is $A_{sc} = 1.66\ m^2$ [*Gurnett et al.*, 1983]. The particles are assumed to be on Keplerian orbits. The relative speed between the spacecraft and the particles is $U = 13.82$ km/s. Solving (7) for n, the impact rates can be converted to number densities. The number density profile is shown at the top of Figure 9 and acquires a maximum value of approximately 0.015 particles per cubic meter, which corresponds to average interparticle distances of the order of a few meters. Concerning the accuracy of the number density values, it can be stated that there is little uncertainty in any of the quantities involved. The statistical error in the counting rate is only a few percent, and the spacecraft velocity relative to the dust grains is known to within a small fraction of a percent. The greatest uncertainty arises in the estimate of the effective area of the spacecraft. It does not include, for example, the large high-gain antenna, which is made of composite material that has a very low yield constant [*Gurnett et al.*, 1983]. The effective area is believed to be accurate to about 10–20%, which makes the number density estimate of comparable uncertainty.

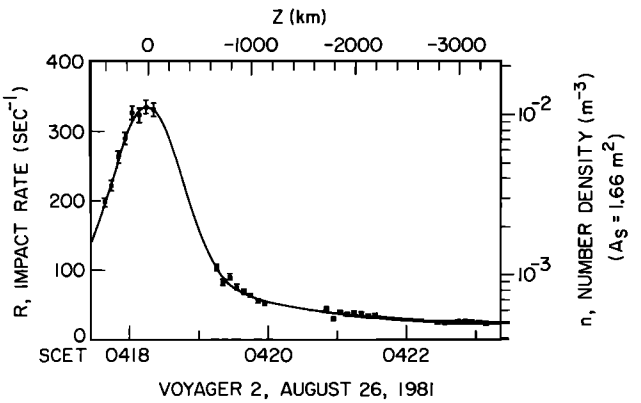

Figure 8. The impact rate R from the wideband receiver and the best fit Gaussian profile (solid line). Note that R acquires its maximum value almost exactly at the equator crossing ($z = 0$). The error bars are 1 σ.

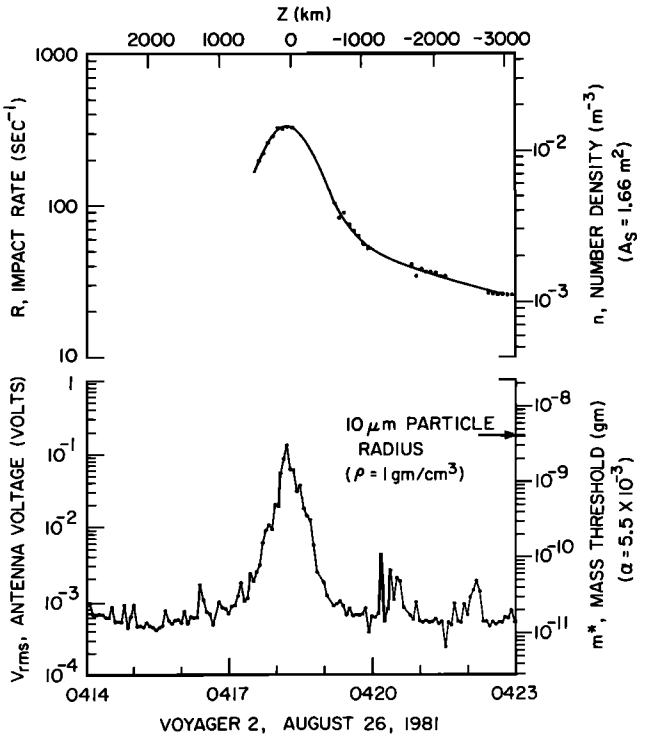

Figure 9. Comparison of the impact rate R and the rms antenna voltage V_{rms}. R and V_{rms} can be analyzed to give the number density n and the mass threshold m^*, respectively. The latter quantities can be seen on the right.

Next we consider the mass threshold of the particles detected by the spacecraft. By combining (1) and (2) the mass can be related to the amplitude of the antenna voltage pulse via the relation

$$m = \left(\frac{C_A}{\alpha k}\right) V. \tag{8}$$

In the wideband receiver the automatic gain control continuously adjusts the gain in order to maintain a nearly constant rms output voltage. This results in the threshold voltage V^*, the lowest voltage for detecting an impact, being directly proportional to the antenna rms voltage V_{rms}, or

$$V^* = \beta V_{rms}, \tag{9}$$

where $\beta = 0.51$, as it was estimated by *Gurnett et al.* [1983]. The combination of (8) and (9) gives the mass threshold m^* for counting particles

$$m^* = \left(\frac{\beta C_A}{\alpha k}\right) V_{rms}. \tag{10}$$

The constants are $\beta = 0.51$, $C_A = 90$ pF, $\alpha = 0.0055$, and $k = 0.21$ C/g. The rms antenna voltage $V_{\rm rms}$ is plotted in the bottom panel of Figure 9, which is the integrated spectrum of the 16-channel spectrum analyzer. The $V_{\rm rms}$ values can be seen on the left of the figure and the m^* values on the right. At the time of the maximum impact rate the mass threshold for counting impacts is seen to be approximately 5.4×10^{-9} g. It should be noted that the mass threshold m^* varies continuously during the equator crossing owing to the fact that the gain of the wideband receiver changes inversely with the rms voltage signal on the antenna. The mass threshold during the crossing varied from about 10^{-11} to 5.4×10^{-9} g. At the peak the number density is $n_{\rm max} \sim 0.015$ m^{-3}, which includes only particles greater than 5.4×10^{-9} g. For a mass density of 1 g/cm^3 (typical dielectric particle, i.e., ice) the resulting radius is 10.9 microns. Denser particles (i.e., silicates where $\rho = 2$ g/cm^3) would have smaller radii (8.7 microns), and fluffy, less dense particles would have larger radii. Despite the fact that the uncertainties for α and k are quite high, the particle size varies as the cube root of these quantities. Therefore the uncertainty of the particle size is reduced by a factor of 2 or 3 accordingly.

A more quantitative way of calculating the particle mass can be obtained from the rms antenna voltage. We assume that the waveforms consist of rectangular pulses of amplitude V_n and duration τ_n. The rms antenna voltage averaged over some time interval T is given by

$$V_{\rm rms}^2 = \frac{1}{T} \sum_n V_n^2 \tau_n, \tag{11}$$

and by using (8) it can be shown that

$$V_{\rm rms}^2 = \left(\frac{\alpha k}{C_A}\right)^2 \frac{1}{T} \sum m_n^2 \tau_n. \tag{12}$$

The pulse durations vary somewhat. These variations, however, are too small compared with the amplitude variations, which means that the pulse duration can be treated as constant, thus $\tau_n = \tau$. The averaging time interval T can also be expressed in terms of the total number of impacts N, as $N = RT$ so that (12) becomes

$$V_{\rm rms}^2 = \left(\frac{\alpha k}{C_A}\right)^2 R\tau \left[\frac{1}{N} \sum m_n^2\right]. \tag{13}$$

The quantity in the brackets is just the rms mass squared, so (13) is finally written as

$$m_{\rm rms} = \left(\frac{C_A}{\alpha k}\right) \frac{1}{(R\tau)^{1/2}} V_{\rm rms}. \tag{14}$$

At maximum impact rate ($R = 334$ s^{-1}) $V_{\rm rms} = 0.137$ V, and using $\tau = 1$ ms and the previous values for the rest of the quantities, we find that $m_{\rm rms}^{\rm max} = 1.8 \times 10^{-8}$ g, which for typical ice particles results in a radius of 16.4 μm.

Comparing the top and bottom panels of Figure 9, it can be seen that the impact rate and the $V_{\rm rms}$ profiles are not identical. More and larger fluctuations take place in the voltage profile, and the impact rate profile is not as sharply peaked as the rms antenna voltage profile. The difference in fluctuations is attributed to statistics. The sample rate of the wideband data receiver is 28,800 samples per second, while the sample rate of the 16-channel spectrum analyzer is 4 samples per second. For this reason, the statistical fluctuations of the impact rate are expected to be much smaller than the fluctuations in the rms antenna voltage. The differences in the shapes of the profiles are attributed by *Gurnett et al.* [1991] to the changes of the mass of the particles.

5. Discussion

In this report we described and analyzed the observations of dust impacts on Voyager 2 during the Saturnian ring plane crossing. The method used was similar to the one that *Gurnett et al.* [1987] used. The new addition was that a new, more accurate value for the charge collection coefficient was used. We are more confident with the new value of alfa and, consequently, with the new results. Our results indicate that the impulses detected by the plasma wave instrument were caused by particles with radii of the order of 10 μm. The mass threshold for detecting these particles changes from 10^{-11} to 5.4×10^{-9} g, and the maximum rms mass of the grains is estimated to be $m_{\rm rms}^{\rm max} = 1.8 \times 10^{-8}$ g. The number density reached a maximum value of about 0.015 particles/m^3, which occurred only approximately 8 km after the equator crossing. The results indicate that there is a dense "disk" of dust particles whose plane, for all practical reasons, coincides with the equatorial plane. The north-south thickness of the impact region is $2\Delta z = 962$ km, based on the first Gaussian fit. Superimposed on this is a less dense "halo" whose north-south thickness is $2\Delta z = 3376$ km, based on the second Gaussian fit.

Gurnett et al. [1983] concluded that the particle sizes ranged from 0.3 to 3 μm. Our new values are considerably higher. The change can be attributed to the new lower estimates of the collection coefficient α. The new α also accounts for the differences in the threshold mass m^*. *Gurnett et al.* [1983] estimated the effective ring thickness to be 106 km by using a mass distribution function. The new thickness of the disk is $2\Delta z = 961$ km. The difference is attributed to the new α value and to the definition of thickness. The authors defined the thickness to be the distance which, when multiplied by the peak particle density, gave the total number of particles per unit area. In our study the disk and the halo thickness estimates result from a Gaussian fit. If we consider the halo thickness ($2\Delta z = 1376$ km), then our results are the same with those of *Warwick et al.* [1982] and *Scarf et al.* [1982]. This is not surprising because both our method and theirs take as thickness the region over which a substantial number of particles could be detected. A study is currently under way in order to validate the method used by *Gurnett et al.* [1983] for deriving the particle mass distribution function and also to derive such functions for Uranus and Neptune.

In the vicinity of Saturn, electromagnetic interactions arise due to the fact that small dust grains become charged by photoemission and electron collection from the ambient plasma. We performed simulations in order to see how the orbit of a charged particle varies owing to the magnetic and gravitational fields of Saturn. The zonal harmonic magnetic field was used, and the oblateness of the planet was included as well [*Connerney et al.*, 1982]. The simulations showed that the motion of larger particles, as seems to be the case in the region sampled by Voyager 2, is almost entirely dominated by gravitational forces; the particles seem to be

confined in the same radial distance they started from; and no substantial latitudinal nor longitudinal excursions occur. Since the particles are large enough and since there is no substantial tilt of the magnetic field, the above results were not surprising. If the particles, however, are smaller than a few microns, then electromagnetic effects become more important [*Schaffer and Burns*, 1987; *Northrop and Hill*, 1983; D. Hamilton, personal communication, 1992].

Voyager 2 crossed the equatorial plane at 2.86 R_S, very close to the G ring. Most likely, the dust particles that were detected by the plasma wave instrument are connected with this ring. By using the best fit Gaussian rate profiles or equivalently, the number density profiles, the columnar number density perpendicular to the equator plane can be computed. The columnar number density κ can be shown to be $\kappa = \pi \int n\, dz$ where n is the particle number density calculated from (6) and (7) and z is the vertical distance. The integration was performed for about 4000 km along the Voyager 2 trajectory centered at the equatorial plane crossing. This was in agreement with the widths of the Gaussian functions given by (6). It was found that $\kappa = 1.51 \times 10^4$ particles/m^2. The constant term R_0 has been ignored since it is smaller than R_1 and R_2, and there is no way to evaluate the thickness associated with this term. From the columnar number density we proceed to calculate the optical depth τ, which is basically a measure of the fraction of the area covered by particles along the column. The optical depth is defined as $\tau = \int nA\, dz$, where A is the area of the particle. Spherical particles were assumed for the calculation. It was found that $\tau = 1.06 \times 10^{-6}$. This is a very small value. The reader should keep in mind that this value is underestimated because it doesn't include small particles below the counting threshold. Recently, *Showalter and Cuzzi* [1993] presented an extended photometric study of Saturn's G ring. They derived a steep particle size distribution function (it varies as r^{-6}). According to their method, an upper limit of about 5×10^{-7} can be placed on the optical depth value for the region that was sampled by Voyager 2 (M. Showalter, personal communication, 1993). Our value is somewhat higher than the value of the photometric study by a factor of 2. The discrepancy is not an alarming one. A possible explanation is that the region sampled by Voyager 2 may exhibit unusual properties. The PWS instrument is sensitive to local properties (at least for the case of dust), whereas the photometric study of *Showalter and Cuzzi* [1993] measures global properties. It is unlikely that the G ring consists of something other than ice, since the primary component of Saturn's rings is ice [*Showalter and Cuzzi*, 1993]. Hence a different composition of particles is ruled out as a reason to account for the discrepancy in the optical depth calculations. Another alternative might be the uncertainty concerning the estimation of k. Since we do not know the yield constant for water ice, k had to be estimated from other materials and could be off by up to a factor of 3 or more. We expect the discrepancy issue is going to be resolved by the upcoming Cassini mission where both the cosmic dust analyzer and the PWS instruments are going to provide measurements of the dust environment of the planet. *Gurnett et al.* [1983] calculated the optical depth to be larger than the optical depth of the current study by an order of magnitude. They derived the optical depth values by using the mass distribution function. The difference in the optical depth values of the current study and of the study by Gurnett et al. is attributed to the value of the charge collection coefficient used. In fact, when the new charge collection coefficient value is used in their approach, τ becomes unacceptably large (about 5×10^{-3}).

Particles of similar size to those detected at Saturn are destroyed relatively quickly, i.e., within a few thousand years, as a result of shattering by collisions and sputtering by magnetospheric ions [*Burns et al.*, 1984]. This seems to be the case for all outer planets. Since the dust grains are lost so quickly, there must be a suitable source for particle production. The G ring, particularly because of its proximity to the spacecraft trajectory, seems to be a very appealing source. Micrometeoroid bombardment of relatively large ring particles produce small dust grains that diffuse outward. Also, nearby moons might contribute to particle production, i.e., Atlas, 1980S27, 1980S26, Janus, Epimetheus, and Mimas whose radial distances vary from 2.28 R_S to 3.08 R_S. We would like to emphasize the fact that the $r_{\text{rms}} = 16.4$ μm value for the particle size is an upper limit. It is a certainty that smaller particles also exist in that area. These particles are not being detected because the voltage they are able of inducing is below the threshold that the PWS can record. If the instrument were able to detect all particles, then the total number of impacts N would have been larger, resulting in a smaller V_{rms} value in (13) and, consequently, a smaller m_{rms} value in (14). Other processes, like solar radiation pressure, electrostatic breakup, stochastic charge variations or charge variations due to planetary shadow, etc., might be responsible for transferring particles from even larger distances. The same processes might replenish particles from the region of interest. Radiation pressure, for one, has a noticeable effect on the eccentricities of smaller particle orbits (D. Hamilton, personal communication, 1992). It seems that there are both a source and a sink of particles in the location that was sampled by Voyager 2. All of the above suggest that the Saturnian G ring is a very dynamic system.

Acknowledgments. The authors would like to acknowledge very helpful discussions with Doug Hamilton, Mark Showalter, Dan Sheehan, Steve Remington, and James A. Van Allen. We would like to thank Mike Kaiser for providing the planetary radio astronomy data which were used in order to establish α for all three outer planetary encounters by Voyager 2. Thanks, of course, go to Kathy Kurth's magic wand that produced this manuscript. This research was supported through contract 959193 with the Jet Propulsion Laboratory.

The Editor thanks E. Grün and another referee for their assistance in evaluating this paper.

References

Aubier, M. G., N. Meyer-Vernet, and B. M. Pedersen, Shot noise from grain and particle impacts in Saturn's ring plane, *Geophys. Res. Lett.*, *10*, 5, 1983.

Burns, J. A., M. R. Showalter, and G. E. Morfill, The ethereal rings of Jupiter and Saturn, in *Planetary Rings*, edited by R. Greenbery and A. Brahic, p. 200, University of Arizona Press, Tucson, 1984.

Connerney, J. E. P., N. F. Ness, and M. H. Acuna, Zonal harmonic model of Saturn's magnetic field from Voyager 1 and 2 observations, *Nature*, *298*, 44, 1982.

Fechtig, H., E. Grün, and J. Kissel, Laboratory simulations, in *Cosmic Dust*, edited by J. A. M. McDonnell, p. 607, John Wiley, New York, 1978.

Grün, E., Impact ionization from gold, aluminum, and PCB-Z, the Giotto spacecraft impact induced plasma environment, *Eur. Space Agency Spec. Publ., ESA SP-155*, 81, 1984.

Gurnett, D. A., E. Grün, D. Gallagher, W. S. Kurth, and F. L.

Scarf, Micron sized particles detected near Saturn by the Voyager plasma wave instrument, *Icarus*, *53*, 236, 1983.

Gurnett, D. A., W. S. Kurth, F. L. Scarf, J. A. Burns, J. N. Cuzzi, and E. Grün, Micron-sized particles detected near Uranus by the Voyager plasma wave instrument, *J. Geophys. Res.*, *92*, 14,959, 1987.

Gurnett, D. A., W. S. Kurth, L. J. Granroth, S. C. Allendorf, and R. L. Poynter, Micron-sized particles detected near Neptune by the Voyager plasma wave instrument, *J. Geophys. Res.*, *96*, 19,177, 1991.

Lee, Y. W., Analytical determination of correlation functions and power density spectrums of random processes, in *Statistical Theory of Communication*, p. 219, John Wiley, New York, 1960.

McDonnell, J. A. M., Microparticle studies by space instrumentation, in *Cosmic Dust*, edited by J. A. M. McDonnell, p. 113, John Wiley, New York, 1978.

Meyer-Vernet, N., M. G. Aubier, and B. M. Pedersen, Voyager 2 at Uranus: Grain impacts in the ring plane, *Geophys. Res. Lett.*, *13*, 617, 1986.

Northrop, T. G., and J. R. Hill, The adiabatic motion of charged dust grains in rotating magnetospheres, *J. Geophys. Res.*, *88*, 1, 1983.

Pedersen, B. M., N. Meyer-Vernet, M. G. Aubier, and P. Zarka, Dust distribution around Neptune: Grain impacts near the ring plane measured by the Voyager planetary radio astronomy experiment, *J. Geophys. Res.*, *96*, 19,187, 1991.

Press, W. H., B. P. Flannery, S. A. Teukolsky, and W. T. Vetterling, *Numerical Recipes (FORTRAN)*, chap. 14, p. 498, Cambridge University Press, New York, 1989.

Scarf, F. L., and D. A. Gurnett, A plasma wave investigation for the Voyager mission, *Space Sci. Rev.*, *21*, 289, 1977.

Scarf, F. L., D. A. Gurnett, W. S. Kurth, and R. L. Poynter, Voyager 2 plasma wave observations at Saturn, *Science*, *215*, 287, 1982.

Schaffer, L., and J. A. Burns, The dynamics of weakly charged dust: Motion through Jupiter's gravitational and magnetic fields, *J. Geophys. Res.*, *92*, 2264, 1987.

Sheehan, D. P., C. A. Casey, and L. T. Volz, Interaction of an expanding plasma cloud with a simple antenna: Application to anomalous voltage signals observed by Voyager 1, Voyager 2, ICE, and Vega spacecraft, *J. Geophys. Res.*, in press, 1994.

Showalter, M. R., and J. N. Cuzzi, Seeing ghosts: Photometry of Saturn's G ring, *Icarus*, *103*, 124, 1993.

Warwick, J. W., D. R. Evans, J. H. Romig, J. K. Alexander, M. D. Desch, M. L. Kaiser, M. Aubier, Y. Leblanc, A. Lecacheux, and B. M. Pedersen, Planetary radio astronomy observations from Voyager 2 near Saturn, *Science*, *215*, 582, 1982.

S. C. Allendorf, L. J. Granroth, D. Gurnett, W. S. Kurth, and D. Tsintikidis, Department of Physics and Astronomy, University of Iowa, Van Allen Hall, Iowa City, IA 52242-1479. (e-mail: Internet: allendorf@iowave.physics.uiowa.edu; Internet: larry-granroth@uiowa.edu; Internet: gurnett@iowave. physics.uiowa.edu; SPAN: iowave::kurth; Internet: tsintikidis@iowave.physics.uiowa.edu)

(Received March 15, 1993; revised August 27, 1993;
accepted October 11, 1993.)